Smart Materials and Structures

PAPER

Self-sensing piezoelectric composite structures leveraging dispersed electro–mechanical impedance spectral measurements

To cite this article: Shulong Zhou *et al* 2025 *Smart Mater. Struct.* **34** 075019

IOP Publishing Smart Materials and Structures
Smart Mater. Struct. **34** (2025) 075019 (15pp) https://doi.org/10.1088/1361-665X/ade91f

Self-sensing piezoelectric composite structures leveraging dispersed electro–mechanical impedance spectral measurements

Shulong Zhou[1], **Yanfeng Shen**[1,*], **Chunquan Wang**[2], **Bao Wang**[2] **and Yuan Tian**[2]

[1] University of Michigan-Shanghai Jiao Tong University Joint Institute, Shanghai Jiao Tong University, Shanghai 200240, People's Republic of China
[2] Wuxi City Huifeng Electronic. Co. Ltd, Wuxi 214100, People's Republic of China

E-mail: yanfeng.shen@sjtu.edu.cn

Received 6 March 2025, revised 6 June 2025
Accepted for publication 27 June 2025
Published 10 July 2025

Abstract

This paper presents a new piezoelectric composite material integrating with dispersed electro–mechanical impedance (EMI) measurements for achieving structural self-awareness. The composite material is meticulously designed and fabricated through homogeneous distribution of piezo-ceramic particulates across an epoxy-based polymeric medium, followed by impregnation into glass fibers. The influence of piezo particles on the mechanical properties of the composite material is systematically investigated through tensile tests. To gain an insight into the EMI active self-sensing integrated with the functional composite structure, finite element modeling is conducted. Subsequently, a root mean square deviation (RMSD) algorithm is adopted for evaluating impedance signal deviations for identifying the damage location. It is found that the RMSD metric indicates substantial deviations in the impedance spectrum near the damage site, while spectra at distant locations show minimal change. Dense electrodes can form dispersed sensing neurons, rendering a high resolution spatial diagnostic capability. Finally, experimental validation is performed, demonstrating the performance of the EMI active sensing for damage diagnostics.

Keywords: smart structures, functional materials, electromechanical impedance spectroscopy, self-sensing, structural health monitoring

1. Introduction

Structural health monitoring (SHM) is an essential technique in structural engineering. It can provide information on structural integrity, thus greatly reducing the probability of catastrophic failure of structures. The emergence of intelligent structures with integrated self-sensing capabilities marks a major advance in structural engineering. These structures have the potential to reduce maintenance costs and prevent major failures. The development of SHM coupled with the integration of self-sensing technology into load-bearing structures could open up a new paradigm for improving the management and safety of infrastructure systems [1].

Piezoelectric materials have both direct and converse piezoelectric effects, allowing them to function as actuation and sensing elements. Among them, piezoelectric wafer active sensor (PWAS) is particularly noteworthy and widely used in SHM applications due to its outstanding performance [2–4]. However, the inherent fragility of these sensors limits their

* Author to whom any correspondence should be addressed.

application. To address this issue, numerous studies have focused on exploring the use of piezoelectric thin films for SHM [5–7]. Chang *et al* developed a novel smart layer for applications in the aerospace field [8]. Additionally, Inman *et al* explored the application of macro fiber composite (MFC) for SHM, broadening the application potential of piezoelectric film technologies in this domain [9, 10]. Taking a similar stance, Yuan *et al* introduced a novel co-curing method for surface mounting, facilitating the *in-situ* incorporation of an extensive sensing network for damage monitoring in intricate structures [11, 12]. Despite these advancements, the installation of sensors remains a critical challenge. Surface-bonded sensors are susceptible to damage from debonding or peeling, which can compromise their long-term performance and reliability. Furthermore, the sensing space resolution is constrained by the number of piezo elements in the system. The increase in sensor density will lead to a dramatic rise in cost.

On the other hand, there is a consensus among researchers that embedding sensors into structures is an alternative approach to achieve structural self-awareness [13, 14]. Minakuchi and Takeda embedded fiber optic sensors for detecting damage, introducing the concepts of 'smart crack arrester' and 'hierarchical sensing system' [15]. Lampani *et al* proposed an embedded self-powered wireless sensor for SHM [16, 17]. Additionally, Sha *et al* designed an embedded smart piezoelectric sensor to extend service life and improve monitoring precision [18]. However, Paget *et al* identified a critical issue through experiments: the low survival rate of embedded piezoceramic transducers within mechanically loaded composite materials [19]. Meanwhile, embedding sensors inevitably causes stress concentrations within materials, potentially initiating local cracks.

Researchers have also explored manipulating material properties to incorporate functional components. Mongioì *et al* designed a stacking laminate by interleaving piezoelectric nanofibers among glass fibers for achieving structural self-sensing [20]. Yin *et al* provided an extensive review about the thermal spray methods in the manufacturing of piezoelectric ceramic coatings, emphasizing their ability to improve the performance and longevity of sensing systems [21]. Philibert *et al* fabricated direct-write piezoelectric transducers by applying sprayed coatings with interdigital electrodes onto carbon fiber composite plates for impact detection [22]. Moreover, researchers have explored the potential of polyvinylidene fluoride (PVDF) as a coating material for SHM. Groo *et al* integrated piezoelectric sensing via acoustic emission testing (AET) with thermally stable DHF PVDF for damage detection [23]. Zou *et al* optimized the blow spinning technology for piezoelectric sensing film, providing a low-cost, self-powered SHM approach [24]. Liu *et al* fabricated PVDF-TrFE transducers for defect detection in multilayer plate via zero group velocity (ZGV) waves [25]. Zhao *et al* developed a self-powered piezoelectric composite, integrating a nanogenerator with traditional composites for self-diagnosis [26]. These approaches mark the forefront of self-sensing structural innovation, yet they also encounter substantial challenges, including the weak actuation capabilities and the constraint to passive monitoring. To address these limitations, pioneering studies have laid a solid foundation for applying piezoelectric composites in SHM. Notably, Raja and Ikeda introduced a novel concept of shear-actuated fiber composites through an electro-elastic model based on a micro-mechanics approach, providing significant insights into optimizing shear actuation and coupling behavior for smart structural applications [27]. Similarly, Raja *et al* contributed a study on the impact of delamination in piezoelectric composite beams and plates, highlighting the degradation of actuator and sensor performance due to damage [28]. Building on these groundbreaking works, developing an innovative multifunctional structure-actuator-sensor system is a crucial approach to advancing self-sensing intelligent structures.

Electro–mechanical impedance spectroscopy (EMIS) has been investigated as a powerful tool for SHM, offering high sensitivity to damage in localized regions of structures. Due to its effectiveness in detecting early-stage material degradation, it has been widely adopted across various structural applications, from aerospace to civil engineering. Giurgiutiu *et al* developed predictive models for EMIS applied to composite materials and conducted damage detection in aging aircraft panels [29, 30]. Park *et al* explored the impedance technology for real-time detection of structural damage in critical civil facilities, particularly in post-earthquake pipeline systems [31]. Raju *et al* highlighted the efficacy of EMIS in conducting thorough and reliable inspections of pipeline systems [32]. Moreover, Li *et al* developed a novel impedance measurement printed circuit board for on-orbit SHM of inflatable structures [33]. Furthermore, Lu and Shen developed the nonlinear EMIS methodology to improve the damage detection sensitivity [34–37]. The present research introduces a novel integration of EMIS with piezoelectric composites, combining the sensing capabilities directly within the material (See figure 1). To the best of the authors' knowledge, this integration has not been previously explored in the existing literature. It facilitates continuous and real-time diagnosis of structural damage, enhancing the robustness, scalability, and accuracy of SHM systems. This integration paves the way for more intelligent and autonomous monitoring solutions in the next generation of smart structures.

This paper proposes an innovative structure-actuator-sensor integration that combines active damage detection with strong mechanical performance. The piezoelectric glass fiber reinforced polymer (GFRP) composite structure is fabricated by distributing the piezo-ceramic powder within epoxy matrix, while utilizing glass fiber reinforcements to enhance the mechanical properties. Electrodes are strategically placed at designated locations to implement a dispersed impedance measurement, enabling the achievement of a high spatial sensing resolution. The finite element (FE) simulations are carried out for damage detection in the proposed composites. Furthermore, an root mean square deviation (RMSD) metric is developed for the damage localization. This composite material integrates its inherent self-sensing capability with the EMIS method,

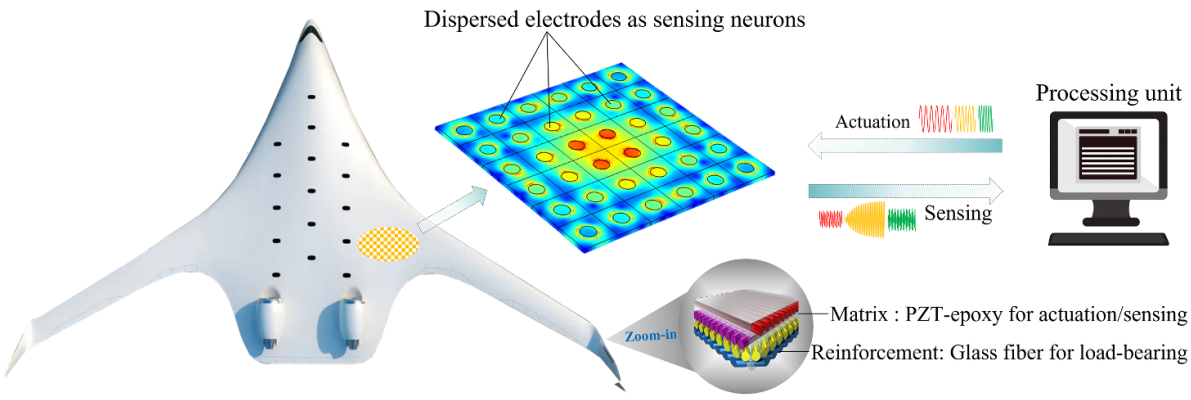

Figure 1. A schematic presentation of self-sensing structural framework with dispersed sensing neurons by high spatial resolution EMI measurements.

overcoming the limitation of traditional self-sensing materials which can only applied for passive monitoring. The proposed approach demonstrates the potential application of this material in aerospace, pressure vessel, and pipeline infrastructure monitoring.

2. Preparation of the piezoelectric composite specimen

This section presents the fabrication process of the piezoelectric composite specimen. Then, a series of experiments are conducted to evaluate the mechanical properties of the composite structure. Finally, the effect of temperature on impedance is studied.

2.1. Design and fabrication of the active composite specimen

For the material preparation, the P-52 ($Pb(Zr_{0.52}Ti_{0.48})O_3$) ceramic powder was chosen as active piezoelectric component. The epoxy resin (SWANCOR 2551) was employed as the bonding matrix, while non-conductive glass fibers (G150) were selected as the reinforcement material. To fabricate the resin, P-52 powder was blended with epoxy resin at a 5:1 weight ratio to ensure optimal piezoelectric functionality.

A systematic preparation method was employed to achieve uniform distribution of PZT powder and minimize agglomeration. The sintered P-52 material was first pulverized using a high-speed grinding device (SHR-10 A) to break down large clusters into finer particles. These particles were then sieved through a precision mesh to remove fragments larger than 0.096 mm, ensuring consistent dispersion within the matrix. The powder was subsequently mixed with epoxy using a vacuum-assisted system to eliminate air voids that could lead to particle clustering. During integration into a woven glass fiber substrate, the mixture was maintained at approximately 40 °C on a thermal platform (DB-C600A) to enhance resin fluidity, thereby improving penetration and reducing interfacial defects. This process resulted in a homogeneous distribution of P-52 particles with no significant aggregation within the composite structure. The structural characteristics and particle distribution were analyzed using scanning electron microscopy (SEM) (VEGA-Compact), as shown in figure 3. The micrograph confirmed an even spread of piezoelectric particles across the matrix, a result of meticulous grinding, sieving, and vacuum-assisted blending. This uniform dispersion was essential for effective load transfer and electromechanical performance, supporting the composite's self-sensing capabilities for SHM applications.

During the manufacturing process, a vacuum extraction method was utilized to eliminate air bubbles within the materials. Figure 3 clearly confirms that the fabricated samples exhibit no significant air bubbles, and the porosity meets the required standards. The presence of pores could disrupt the continuity of the piezoelectric phase, significantly impairing the sensing and actuation capabilities of the piezoelectric composite material. For instance, increased porosity might have diminished impedance signature amplitude, making it challenging to distinguish between pristine and damaged states. In actuation, voids hindered stress transfer between the matrix and piezoelectric particles, limiting mechanical deformation under electric fields. Additionally, voids could have acted as stress concentration points, accelerating degradation under cyclic loadings. By achieving low porosity through refined fabrication techniques, the proposed composite ensured reliable signal transmission and mechanical response, making it highly suitable for distributed sensing and actuation in intelligent structural systems.

The fabrication process employed autoclave molding to achieve high-performance, defect-minimized piezoelectric composites, as illustrated in figure 2. Prepared prepregs were layered inside a mold, sealed to maintain a vacuum environment, and then subjected to a controlled heat and pressure cycle in an autoclave. The curing process initially involved holding the composite at 40 °C for 1 h under a pressure of two bars to allow excess resin to flow and minimize air bubbles, and then a constant temperature 80 °C was held and followed by isothermal retention for 9.5–10.5 h to facilitate

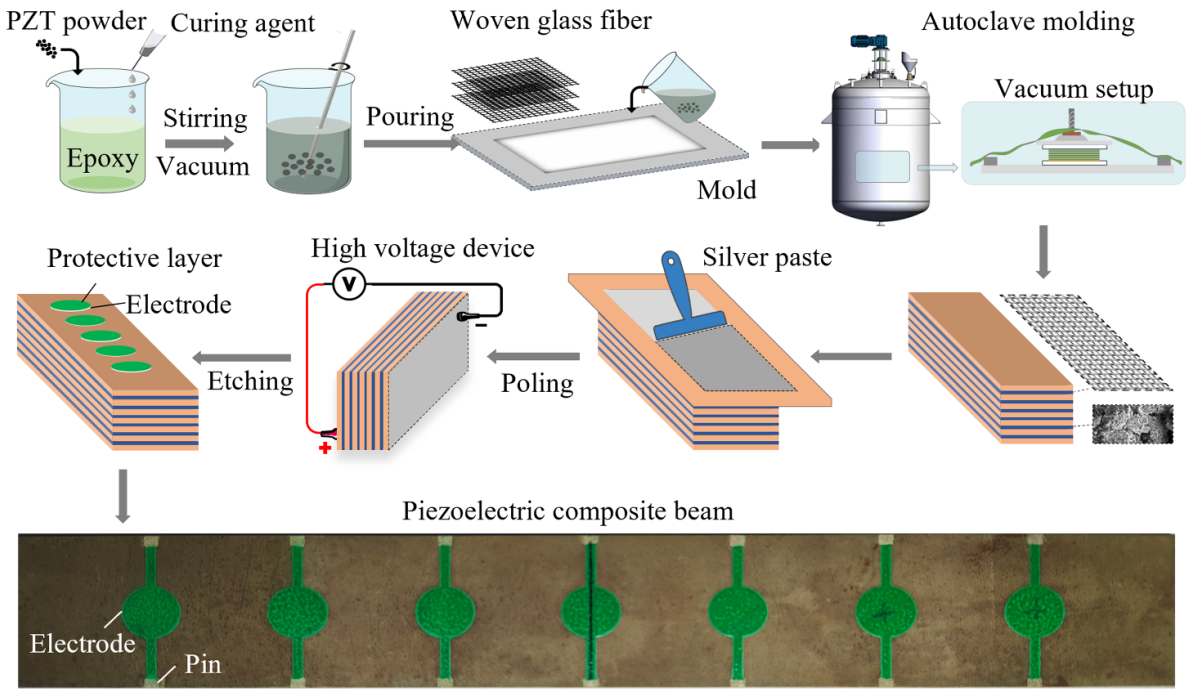

Figure 2. Fabrication procedure for a piezoelectric composite beam.

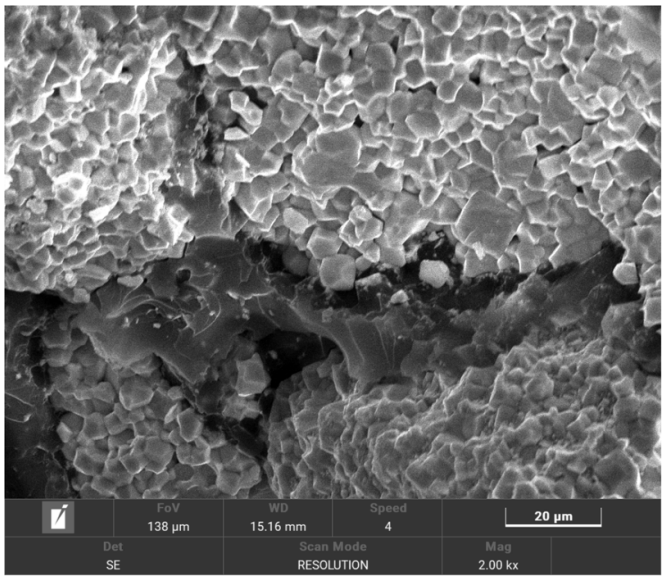

Figure 3. SEM image of the piezoelectric composite.

full cross-linking of the thermosetting matrix. After cooling to room temperature and releasing the pressure, the composites were exposed to a poling condition to induce piezoelectric properties. A patterned conductive layer was deposited via precision screen printing on the surface of the specimen and subjected to a 9 kV mm^{-1} electric field in oil for 15 min, facilitated by a high-voltage amplifier. An iodine-potassium iodide etchant, prepared by mixing iodine (I_2), potassium iodide (KI), and distilled water (H_2O) in a 1:3:16 weight ratio, was utilized for precision silver etching. Excess silver was chemically etched to preserve the electrode pattern, enabling each electrode location to serve as both an actuator and a sensor. The final specimen measuring a size of 200 mm in length, 30 mm in width, and 2 mm in thickness was fabricated, consistent with the numerical simulation setup in section 4.

Conventional electro–mechanical impedance (EMI) sensors that require densely dispersed placement for localized damage detection, the proposed self-sensing piezoelectric composite inherently possessed sensing capability throughout its entire structure. It enabled integrated distributed sensing via customizable electrode patterns printed directly onto the material surface, allowing these electrodes to function as a network of sensing units. By tailoring these patterns, dense sensor arrays can be easily achieved, significantly reducing material, installation, and maintenance costs. Additionally, the composite served a dual purpose of load-bearing and precise damage detection and localization, enhancing its applicability in real-world structural systems such as those in aerospace and automotive engineering, where both structural integrity and health monitoring are paramount.

Table 1 summarizes the measured piezoelectric and electromechanical properties of the developed piezoelectric composite specimen. The piezoelectric constant (d_{33}) was determined to be approximately 32 pC N^{-1}, markedly higher than the typical values of around 20 pC N^{-1} reported for glass fiber-reinforced PVDF polymer composites [38]. Under test conditions (25 °C, 40% relative humidity), the capacitance was recorded at 21 pF, reflecting the composite's dielectric characteristics. Additionally, the dielectric loss factor (tanδ) was measured at 2.35, substantially higher than values observed in conventional piezoelectric ceramics [39]. Moreover, the electromechanical coupling factor (k_{33}) was evaluated at 0.25,

Table 1. Piezoelectric properties of the piezoelectric composite specimen.

Property	Symbol	Unit	Value	Test condition
Piezoelectric constant	d_{33}	pC N^{-1}	32	25 °C and 40% RH
Electromechanical coupling factor	k_{33}	—	0.25	
Capacitance	C	pF	21	
Dielectric loss factor	tanδ	—	2.35	

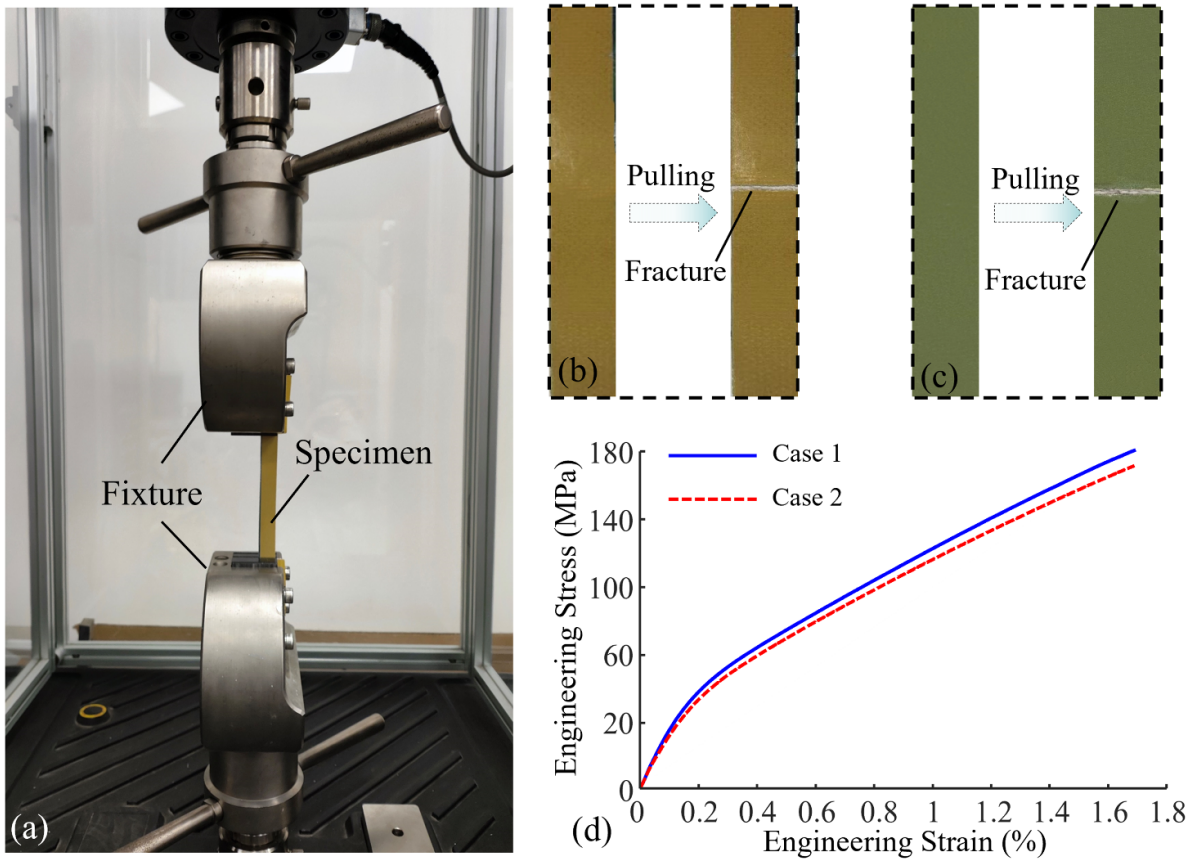

Figure 4. (a) Tensile test experimental setup; (b) case 1 (specimen without piezo-ceramic powder); (c) case 2 (specimen with piezo-ceramic powder); (d) tensile test results.

suggesting limited energy conversion efficiency compared to pure ceramics. These findings highlighted the trade-off between the processability of the composite and its piezoelectric performance.

2.2. Tensile tests on the specimen

Integrating piezoelectric powder into the composite enables the addition of sensing capabilities but simultaneously arose concerns of its influence on the load-bearing capacity. Therefore, it is essential to evaluate whether the smart structures retain adequate mechanical strength. Therefore, two distinct sample configurations were employed for a comparative experimental analysis. Case 1 excluded piezoelectric powder, serving as the comparative base, representing conventional composite structures. Case 2 retained the same material ingredients and fabrication procedure, with the only modification being the incorporation of piezoelectric powder. The specimens were manufactured to measure 120 mm long, 28 mm wide, and 1 mm thick. Under quasi-static loading conditions, the specimens were rigidly constrained within the universal testing apparatus (MTS), employing immobilized terminal fixation and displacement-controlled axial loading. The load was applied at a constant displacement rate of 0.5 mm min^{-1} to ensure smooth and controlled stress application. Throughout the test, the elongation of the specimen and the applied load were continuously monitored via high-precision displacement and load sensors until the specimen fractured. The data were recorded in real-time by a computer system, generating the stress–strain curve. The initial and failed morphologies of the laminated composite specimens were shown in figures 4(b) and (c).

Table 2. Comparison of mechanical properties for conventional and multifunctional composite specimens.

Material	Relatively density, γ	Specific strength S/γ (MPa)	Specific stiffness E/γ (GPa)
Case 1	2.37	79.16	16.54
Case 2	2.72	67.22	12.65

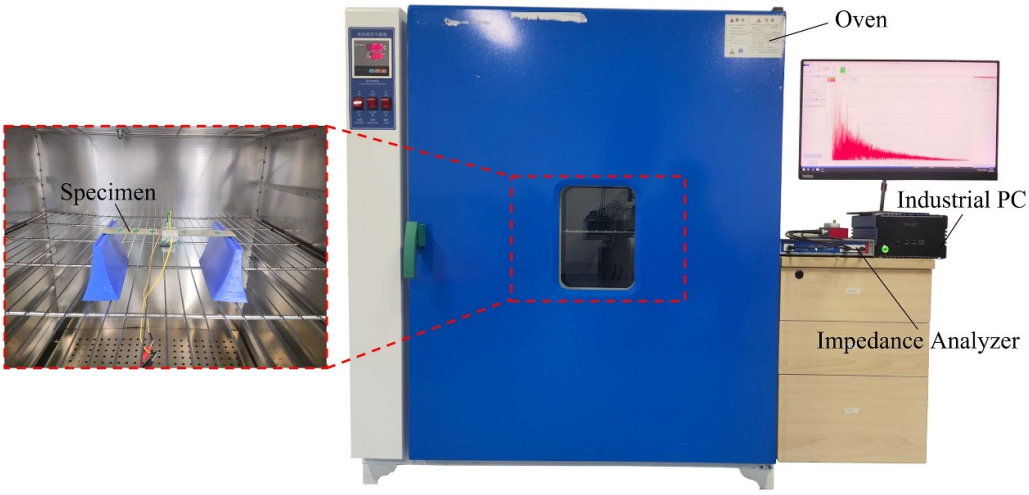

Figure 5. Experimental layout of the temperature tests on the specimen.

Figure 4(d) presents the results from the tensile tests, with the stress-strain curves showing a consistent increase in stress as strain grew for both composite specimens. Table 2 summarizes the key mechanical properties, which are critical for evaluating the material's mechanical performances. The specific strength and specific stiffness of both samples were comparable, with only slight variations observed. The analysis revealed that the incorporation of piezo-ceramic powder led to a slight decrease in ultimate tensile strength and stiffness. However, this reduction was minimal, and the composite retained sufficiently outstanding mechanical properties. This suggested that the material's overall structural performance was largely unaffected by the addition of the piezo-ceramic powder, making it suitable for multifunctional applications where both mechanical strength and self-sensing capabilities were required.

2.3. Temperature tests on the specimen

To investigate the effect of temperature on the impedance response of the developed self-sensing piezoelectric composite structures, a series of controlled experiments were conducted. The primary objective was to quantify variations in impedance spectra under varying thermal conditions. Figure 5 illustrates the experimental setup for the measurement of temperature-dependent EMI responses. A programmable oven (101–4B) maintained temperatures between 20 °C and 70 °C with an accuracy of ±0.5 °C. The piezoelectric composite specimen was mounted on supportive blocks inside the oven to replicate boundary condition used throughout this study, as depicted in figure 5. An impedance analyzer recorded EMI spectra over a frequency range from 20 kHz to 250 kHz at an excitation voltage of 1 V. Tests were conducted at temperatures ranging from 30 °C to 70 °C in 10 °C increments (30 °C, 40 °C, 50 °C, 60 °C, and 70 °C), with data collected at each level after a 20 min stabilization period to ensure thermal equilibrium.

Figure 6 presents the experimental results under varying temperature conditions. The measurement at 30 °C was recorded after thermal cycling as the baseline. Figure 6(b) displays the results of the quantification process used to analyze the impedance response under different temperature conditions. To perform this analysis, the impedance magnitude for each temperature condition was compared to the baseline measurement, calculating a ratio across the entire frequency spectrum as follows:

$$R_T = \frac{\overline{|Z_T|}}{\overline{|Z_{\text{Base}}|}} \tag{1}$$

where $\overline{|Z_T|}$ is the average impedance magnitude at temperature T, $\overline{|Z_{\text{Base}}|}$ and is the average impedance at the baseline temperature of 30 °C. This ratio helped highlight how the impedance changed with temperature relative to the reference condition.

Preliminary findings indicated a notable decrease in impedance magnitude with rising temperature, due to increased dielectric losses ($\tan\delta = 2.35$ at 25 °C, as shown in table 1) and softening of the polymer matrix. Furthermore, performance degradation of the piezoelectric ceramic particles at elevated

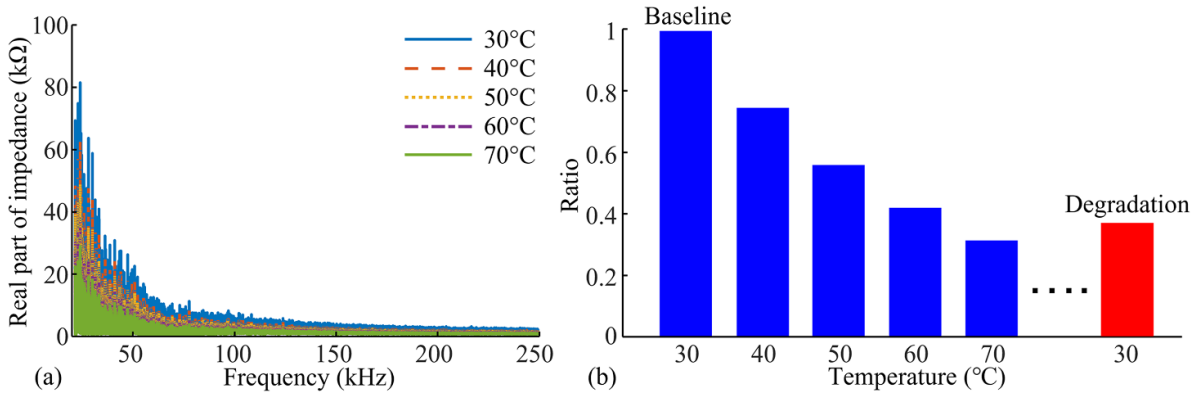

Figure 6. (a) Impedance results at different temperatures; (b) temperature-dependent trend quantification results.

temperatures contributed to this trend, as higher temperatures typically reduced the piezoelectric constant (d_{33}) and electromechanical coupling factor (k_{33}) due to thermal depolarization and enhanced domain wall mobility [40]. It was critical to emphasize that the material exhibited irreversible degradation of piezoelectric performance upon exposure to high temperatures, as shown in figure 6(b). But it still can provide meaningful impedance peaks. These results were consistent with prior studies, illustrating the thermal effect on the piezoelectric properties [41–43].

3. EMIS method integrating with piezoelectric composite structures

The EMIS method relies on frequency-domain measurements through discrete, incremental frequency sweeping. Sinusoidal excitations applied at the electrode terminal induce steady-state electro-mechanical responses, with actuation and sensing occurring concurrently to derive precise impedance values for each frequency. These excitations generate elastic waves that interact with the material's microstructure and boundaries, creating localized vibrational modes. In contrast to conventional bursts of propagating Lamb waves, EMIS responses are dominated by continuous and standing Lamb waves. Formed by the interference of reflected waves at boundaries or discontinuities within a composite laminate, these standing waves produce resonant patterns at specific frequencies. EMIS emphasizes on localized resonance sensitivity to nearby structural changes like localized cracks, delamination, or material degradation, enabling accurate damage detection via impedance signatures in distributed sensing applications.

In conventional setups, a single PWAS transducer often functions as both the actuator and the receiver, either adhered to or embedded within the structure to capture resonant characteristics [30, 44]. However, this approach faces challenges related to external sensor placement, maintenance, and inconsistent coupling conditions, which could compromise monitoring reliability and hinder accurate structural health assessment. To address these limitations, this research integrates the EMIS method with piezoelectric composite materials, utilizing a diversified and customizable design of distributed sensing electrodes. This innovative approach eliminates the need for external sensors, as the composite inherently supports self-excitation and self-sensing, as depicted in figure 7. Custom electrode patterns printed on the composite surface enable designated regions to apply electrical actuation, leveraging the material's piezoelectric properties for immediate electro–mechanical feedback.

For real-time application in online SHM, the system is engineered for continuous operation under dynamic conditions. Unlike traditional offline methods, this online SHM functionality enables real-time damage identification without requiring equipment downtime, thereby minimizing operational interruptions in critical sectors such as aerospace and automotive structures. Furthermore, the distributed sensing scheme significantly enhances the spatial resolution of damage detection.

4. Numerical investigation of EMI active sensing

In this section, the FE models are conducted integrating the EMIS method for diagnosing structural damage. Subsequently, the RMSD metric is proposed for the damage localization.

4.1. Numerical modeling

The FE simulations were performed using ANSYS 16.0. Based on the experimental measurements, the density of the piezoelectric composite material was 2720 kg m^{-3}. The key material properties were determined through experimental testing of actual composite specimens, accurately simulating the electro–mechanical behavior of the piezoelectric composite. The specific coefficients

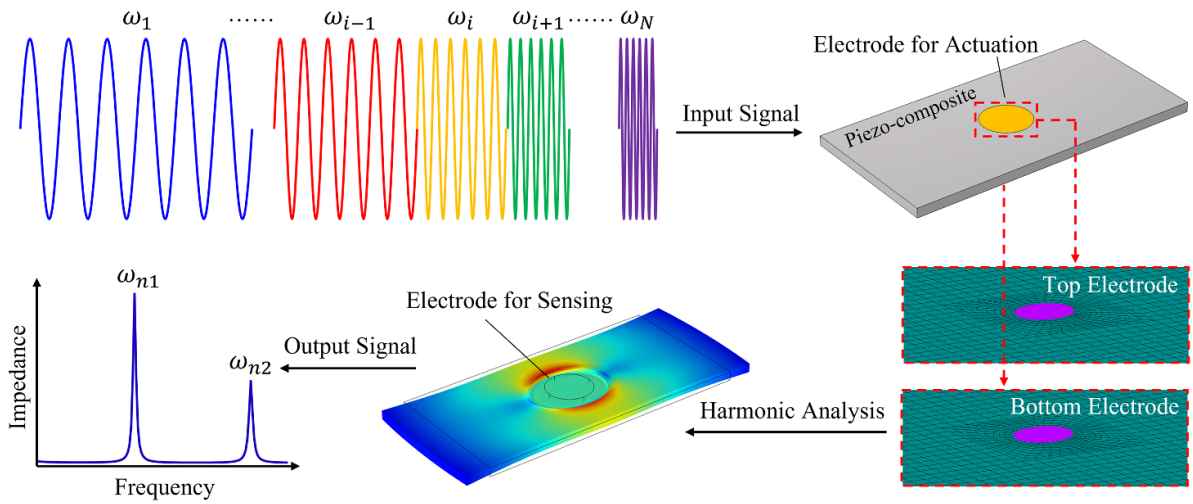

Figure 7. Illustration of the EMIS method on a piezoelectric composite structure.

used in the model are detailed below:

$$[C_p] = \begin{bmatrix} 37.22 & 9.63 & 9.63 & 0 & 0 & 0 \\ 9.63 & 37.22 & 9.63 & 0 & 0 & 0 \\ 9.63 & 9.63 & 5.101 & 0 & 0 & 0 \\ 0 & 0 & 0 & 2.083 & 0 & 0 \\ 0 & 0 & 0 & 0 & 13.76 & 0 \\ 0 & 0 & 0 & 0 & 0 & 13.76 \end{bmatrix} \text{GPa} \quad (2)$$

$$[e_p] = \begin{bmatrix} 0 & 0 & -5.203 \\ 0 & 0 & -5.203 \\ 0 & 0 & 15.08 \\ 0 & 0 & 0 \\ 0 & 12.718 & 0 \\ 12.718 & 0 & 0 \end{bmatrix} \text{C m}^{-2} \quad (3)$$

$$[\varepsilon_p] = \begin{bmatrix} 182.87 & 0 & 0 \\ 0 & 182.87 & 0 \\ 0 & 0 & 159.45 \end{bmatrix} \quad (4)$$

where $[C_P]$ refers to the stiffness matrix; $[e_P]$ indicates piezoelectric matrix; $[\varepsilon_P]$ denotes the dielectric matrix.

To reduce the computational burden and modeling complexity of multilayer composite structures, the equivalent material model was utilized. It treated the structure as a homogenized material with effective properties, rather than modeling each layer individually. It reduced computational cost while preserving reasonable accuracy in representing the overall structural response. The three-dimensional FE models displayed in figure 8 are employed to simulate the EMI active sensing procedure. SOLID226 elements were deployed to discretize the entire piezoelectric composite beam, which measured with the identical dimensions to the actual specimen. The impact of local damage on the impedance response was evaluated using such a model. An in-plane mesh refinement of 1 mm was utilized to optimize the trade-off between numerical precision and computational burden. The sensing electrodes were designed with a diameter of 10 mm and arranged on both the top and bottom surfaces of the beam. The spacing between the electrodes was set to 25 mm to ensure adequate coverage for monitoring large areas, while the specific arrangement was designed to enable precise detection of localized structural damage.

Structural stiffness reduction in local areas was employed to represent general damage sites within the structure. This method simulated the degradation of mechanical properties in laminated composite structures caused by a general damage representative, which could be matrix cracking, delamination, or fiber pull-out for resulting in such a stiffness reduction effect. In the SHM research community, this method was widely employed for studying the general damage effect on the response signals [45, 46]. As shown in figures 8(b) and (c), the damages were placed at specific locations. The first damage was positioned between electrodes #3 and electrodes #4, while the second damage was placed between electrodes #6 and electrodes #7. Using the impedance signals of all electrodes in the undamaged model as a baseline, a comprehensive analysis and evaluation of impedance variations under damaged conditions were conducted.

4.2. Analysis of simulation results

The selection of the appropriate range of the sweeping frequency band can considerably influence the efficacy of the damage detection employing the EMI technique [47]. The research involved harmonic analysis, where frequencies were swept from 20 kHz to 250 kHz. This was performed in 690 incremental steps to obtain the spectral characteristics. Figure 9 presents the impedance curves at several representative electrodes. In all three cases, electrode #1 was located far from the damage sites, resulting in the minimal variation in its impedance spectra. The impedance spectra of electrode #3 with damage exhibited significant changes compared to its undamaged state, reflecting the direct impact of local damage on the sensing signal. In contrast, the impedance spectra of electrode #7 in figure 9(c) remained consistent under pristine and one damage case. These results suggested that

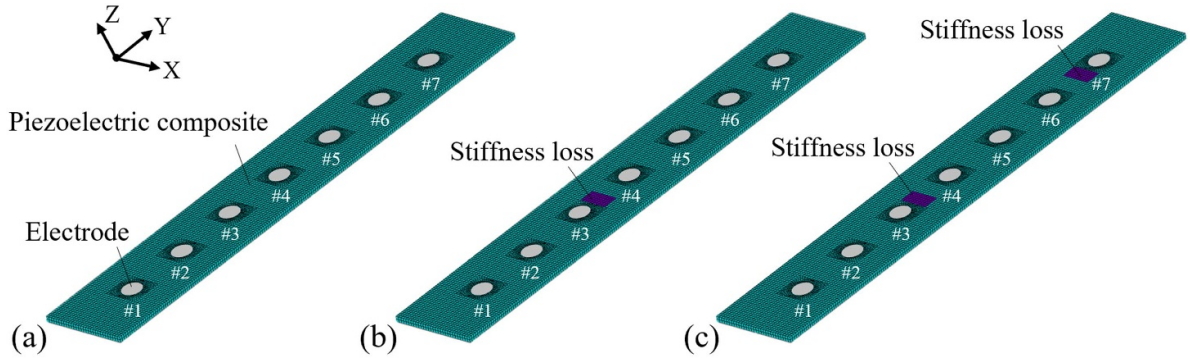

Figure 8. FE models for EMIS active sensing of piezoelectric composite beams: (a) case 1 (pristine case); (b) case 2 (one damage area); (c) case 3 (two damage areas).

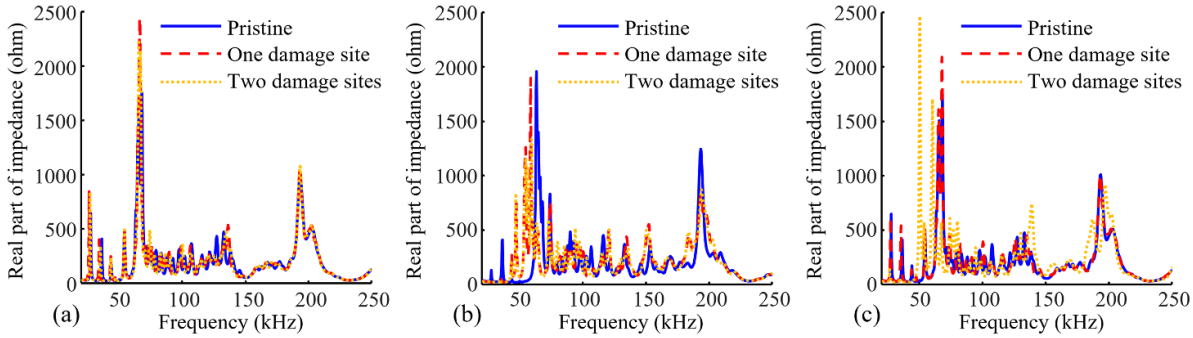

Figure 9. The impedance spectra comparison: signals from (a) electrode #1; (b) electrode #3; (c) electrode #7.

while the impedance spectrum was highly sensitive to damage, its effects were confined to localized regions.

Figure 10 elucidates the snapshots at peak structural resonance from distinct electrodes. When the sensing location was positioned away from any damage, the primary vibrational energy of the resonance was localized in the vicinity of the excited electrode region, as shown in figure 10(a). It was also observed that damage situated far away from the excitation electrode had negligible impact on the stress distribution. In contrary, when the damage area occurred in proximity to excitation electrode, the distribution of equivalent stress was significantly disrupted, forming an irregular high-stress region around the sensing area. This disruption was driven by the shift in resonance frequency caused by the damage, leading to a comprehensive alteration in the overall stress distribution. This evidently offered a visualization for the EMI resonance scenarios. These phenomena aligned with the impedance spectrum characteristics presented in figure 9. The effective damage detection area of a single electrode was validated through the simulation, providing a theoretical foundation for optimizing the distribution design of sensing electrodes in practical applications. In conclusion, EMIS method focused on detecting localized changes in material properties and structural dynamics, which was a key feature for accomplishing active sensing and damage localization of the composite structures.

The results presented in figure 11 depict the impedance curves for each electrode pair for both pristine and damaged conditions. For the undamaged structure, the spectra exhibited a clear symmetry centered around electrode #4 (the central sensing electrode). This symmetric behavior served as a reference baseline, providing insight into the structural integrity of the system. Upon introducing the damage, the spectra of electrodes in close proximity to the damage site indicated significant deviations. Specifically, the shift in the impedance peak and variations in its amplitude were most pronounced in these nearby electrodes. In contrast, electrodes located further from the damage site remained nearly unaffected, as their spectra displayed only minor or negligible changes. This localized behavior aligned closely with the trends observed in figure 9, corroborating the sensitivity of the impedance measurements to damage location. The shift and amplitude changes in the impedance peaks served as key indicators of structural damage.

4.3. Damage localization via RMSD

The RMSD has been predominantly employed as a quantitative metric to assess the congruence between two EMI spectra. It serves as a statistical measurement of the average magnitude of deviation between corresponding impedance values for the structures under comparison. This research employed

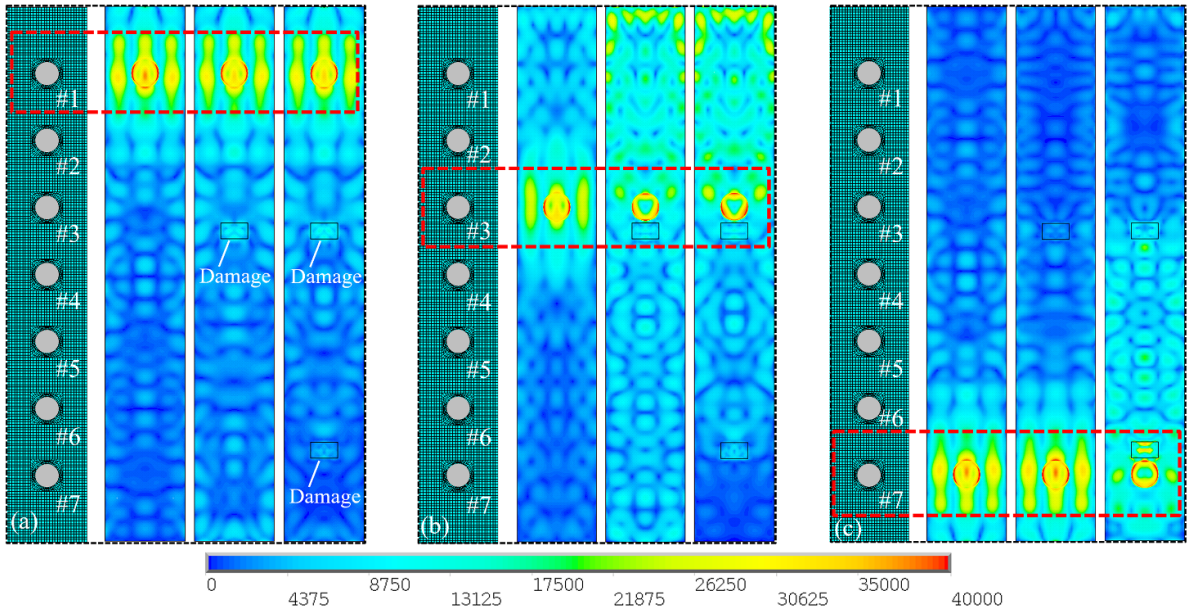

Figure 10. Comparison of the snapshots at structural resonance peaks: active sensing at (a) electrode #1; (b) electrode #3; (c) electrode #7.

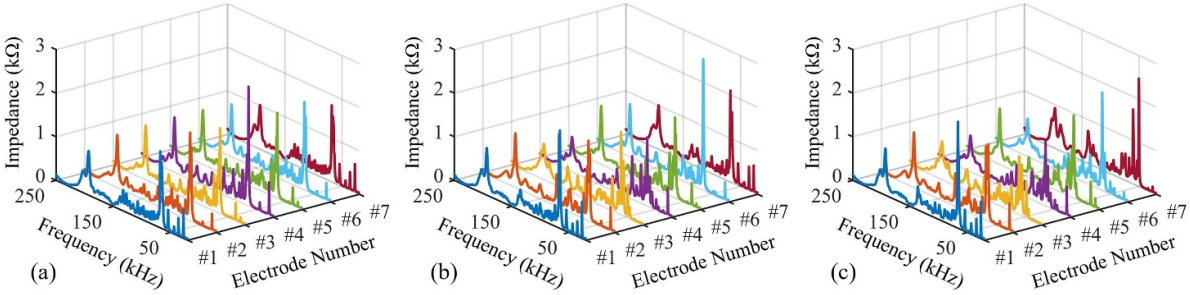

Figure 11. The real part of impedance spectra for different scenarios: (a) case 1 (pristine case); (b) case 2 (one damage area); (c) case 3 (two damage area).

the RMSD damage metric, defined as follows:

$$RMSD = \sqrt{\sum_{i=1}^{n} \left[\mathrm{Re}\left(Z_i\right) - \mathrm{Re}\left(Z_i^0\right)\right]^2 / \sum_{i=1}^{n} \mathrm{Re}\left(Z_i^0\right)^2}. \quad (5)$$

Here, N corresponds to the quantity of frequencies, the 0 indicates the pristine condition, and Z denotes the impedance measurement at the corresponding frequency.

Figure 12 delineates the impedance deviations observed under the damage scenarios. It was revealed that the metric exhibited a high degree of effectiveness in capturing the impedance discrepancies between the case studies. Specifically, the RMSD values associated with the electrodes manifested a pronounced increment in regions adjacent to the damage sites. The spatial distribution of these RMSD values is closely associated with the location of structural damage, indicating that the self-sensing piezoelectric composite structural system not only detects the presence of damage but also provides precise localization of the damage. Moreover, even in the presence of multiple damage sites, the system demonstrated the capability to distinctly identify multiple RMSD peaks. The RMSD peak indicated that even in the presence of two damages, the localization and monitoring of damage could still be effectively achieved.

5. Experimental demonstration of EMI active sensing

This section presents comprehensive experimental investigations for evaluating the efficacy of EMIS in the piezoelectric composite structures. Subsequently, the RMSD metric is also employed for the damage detection and localization.

5.1. Experimental setup

Figure 13 shows the experimental setup. Iron blocks were attached on the surface of the specimen for mimicking the damage sites. In line with the approach taken in the numerical simulations, EMI data were obtained by the impedance analyzer (Omicron Bode 100) to discern subtle changes within the piezoelectric material caused by structural damage sites.

A detachable electrical connection was established using clamps attached to designated electrode pins, providing a reliable and consistent interface for signal transmission while

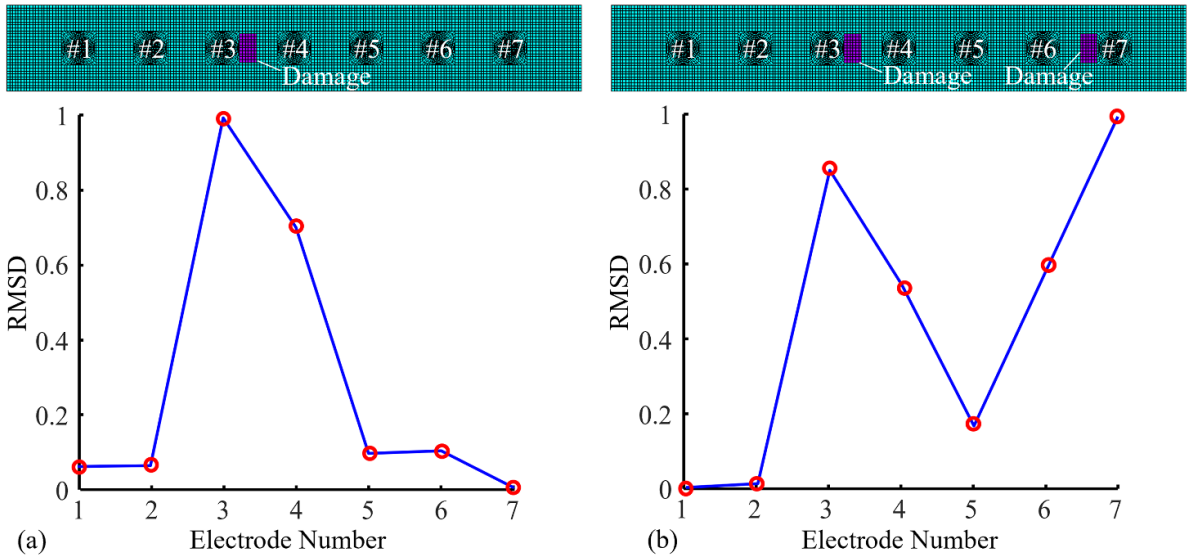

Figure 12. RMSD for the damage cases: (a) one damaged area; (b) two damaged areas.

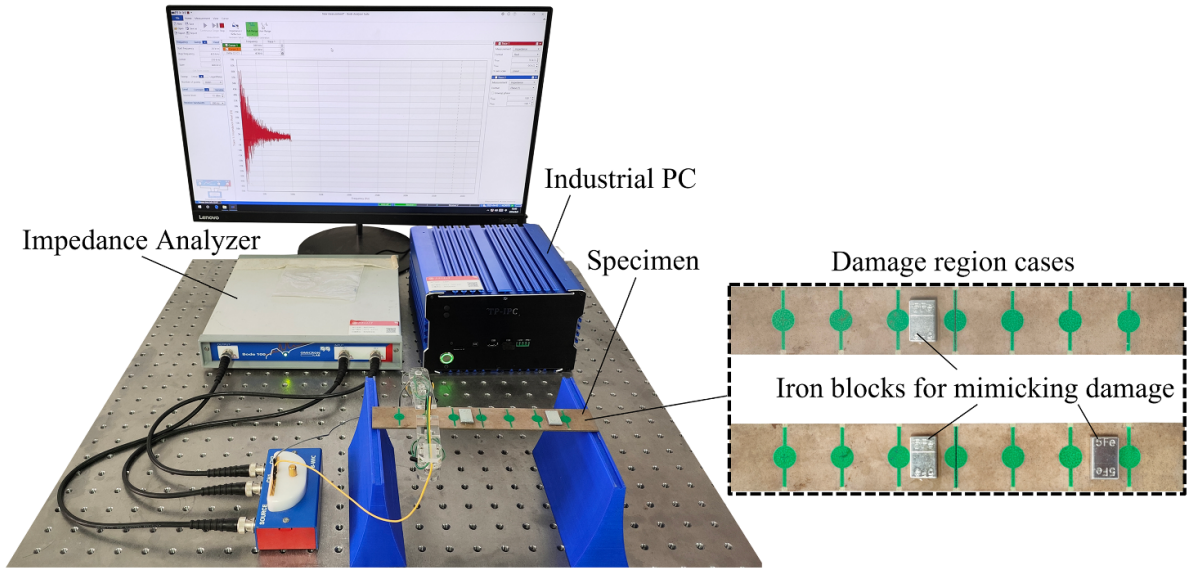

Figure 13. The experimental setup for demonstrating self-sensing of composite beams.

facilitating ease of assembly and disassembly. Previous studies have explored and demonstrated the sensitivity of EMI signals to boundary and loading conditions in SHM applications. For instance, Giurgiutiu and Zagrai reported notable shifts in resonance frequencies under varying clamping conditions [48], while Soh *et al* highlighted the impact of applied loads on impedance magnitude in composite structures [49]. Thus, two blocks were placed at both ends of the specimen during the experiments to ensure a consistent boundary and loading condition. It should be noted that the focus of this study was to evaluate the active sensing capability of self-sensing piezoelectric composites using the EMIS method under controlled conditions. To ensure result consistency and comparability, all experiments were conducted with identical boundary and loading setups.

5.2. Experimental results and discussion

The impedance spectra obtained from experimental measurements are depicted in figure 14. Owing to the highly intrinsic damping properties of the material in the fabricated sample, the experimentally acquired impedance spectra showed a decreasing amplitude with respect to frequency, deviating from the numerical simulations. Specifically, impedance peaks of the structure were concentrated in the lower frequency domain. This damping effect suppressed higher-frequency resonances and altered the overall dynamic response of the structure. In the baseline (undamaged) condition, the impedance spectra were asymmetrical around the central sensing electrode (electrode 4). This asymmetry arose from minor manufacturing imperfections introduced during the

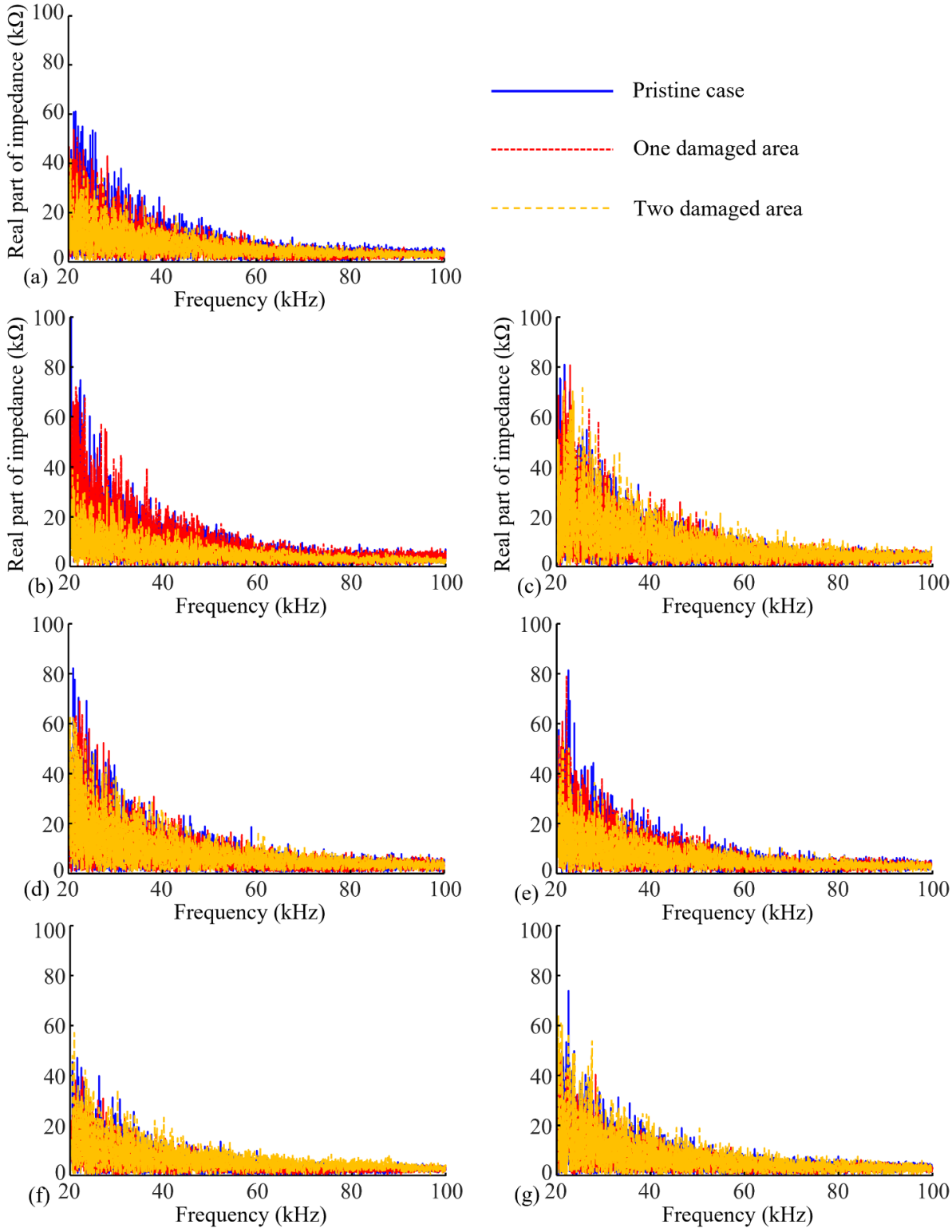

Figure 14. Experimental impedance spectra comparison: (a) electrode #1; (b) electrode #2; (c) electrode #3; (d) electrode #4; (e) electrode #5; (f) electrode #6; (g) electrode #7.

fabrication process, such as slight variations in material properties or geometric dimensions. Despite these discrepancies, the efficacy of subsequent damage monitoring remained unaffected, as long as the baseline signals were accurately obtained.

Experimental validation and analysis confirmed the effectiveness and potential of the proposed self-sensing piezoelectric composite for SHM applications. The RMSD algorithm demonstrated outstanding performance in detecting impedance discrepancies between the pristine and the damaged

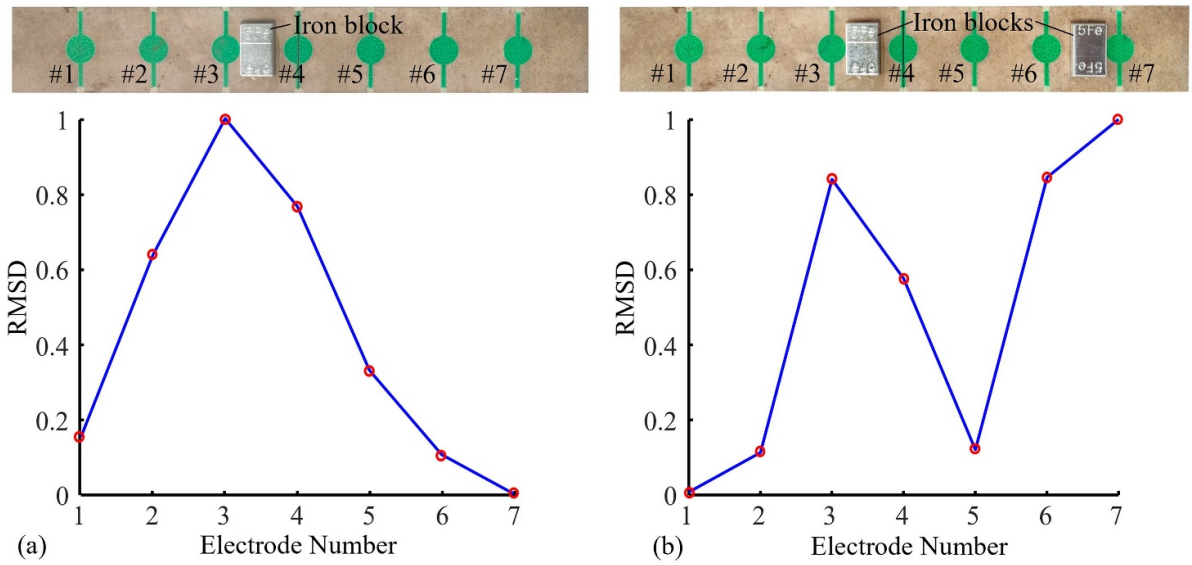

Figure 15. RMSD for the damage cases: (a) one damaged area; (b) two damaged area.

states, as illustrated in figure 15. The RMSD values exhibited significant increases near damage sites in both single and multiple damage scenarios. This electrode configuration not only enhanced the spatial resolution without significantly increasing hardware costs but also allowed for customization of electrode shapes to meet the testing requirements of some specific structures. Compared to conventional sensor networks, the scalability and design flexibility of piezoelectric self-sensing composite materials greatly improved their applicability for practical application, substantially reducing costs associated with hardware and mitigating system complexity issues.

Despite these advantages, it is essential to acknowledge that this method has certain limitations. Firstly, the measurement principle of the EMIS dictates that it exhibits higher sensitivity only to areas in close proximity to the electrodes. Additionally, as demonstrated in section 2.3, environmental factors such as temperature variations may impact the accuracy of the measurements. To address these shortcomings, future research could focus on developing tailored plans for different structures, optimizing the size and shape of sensing electrodes to achieve maximum sensitivity. Moreover, to mitigate the effects of temperature changes, compensation algorithms could be implemented to enhance monitoring consistency. For multi-channel signal acquisition demand, techniques such as multi-sensor data fusion and matrix switch could be employed to reduce hardware costs and system complexity. These improvements would enhance the system's reliability and broaden its applicability in real-world scenarios. These aspects will be explored in a future study.

6. Conclusions and future work

This research proposed an intelligent piezoelectric composite utilizing the EMIS methodology to achieve structural self-awareness and health monitoring. The manufacturing process of the piezoelectric composite structures was described in details, where sample beams were produced through rigorous material optimization and process refinement, ensuring high sensing sensitivity and function reliability. Coupled-field FE models validated the feasibility of employing EMIS for active structural sensing. Experimental validations demonstrated the accuracy and effectiveness of the proposed smart system, demonstrating the prowess of novel composite structural system for establishing self-awareness. Each location of the structure can serve dual roles as both an actuator and a sensor, enabling high-resolution active sensing damage assessments.

Future research will further investigate a bio-inspired physical neuron system in the structures functioning with an artificial neuron network as the sensing algorithm to strive for the next generation of smart structures as a broader and more general solution.

Data availability statement

The data that support the findings of this study are openly available at the following URL/DOI: https://doi.org/10.5281/zenodo.15813204.

Acknowledgments

The support from the National Natural Science Foundation of China (Contract Number 52475161) is gratefully acknowledged. Dr Yanfeng Shen also extends appreciation for the funding provided by John Wu & Jane Sun Endowed Professorship.

References

[1] Soleymani A, Hasani H, Nasseri H R, Azizi M B and Abbasi A H 2022 A review of self-sensing based structural

health monitoring *2nd. Int. Conf. on Architecture, Civil Engineering, Urban Development, and Environment* (*Tabriz, Iran, 27 May 2022*)
[2] Giurgiutiu V 2005 Tuned lamb wave excitation and detection with piezoelectric wafer active sensors for structural health monitoring *J. Intell. Mater. Syst. Struct.* **16** 291–305
[3] Shen Y and Cesnik C E S 2018 Local interaction simulation approach for efficient modeling of linear and nonlinear ultrasonic guided wave active sensing of complex structures *J. Nondestruct. Eval. Diagn. Prognost. Eng. Syst.* **1** 011008
[4] Shen Y and Cesnik C E S 2017 Modeling of nonlinear interactions between guided waves and fatigue cracks using local interaction simulation approach *Ultrasonics* **74** 106–23
[5] Tian R, Nie G, Liu J, Pan E and Wang Y 2021 On Rayleigh waves in a piezoelectric semiconductor thin film over an elastic half-space *Int. J. Mech. Sci.* **204** 106565
[6] Liang F, Liang D-D and Qian Y-J 2020 Dynamical analysis of an improved MEMS ring gyroscope encircled by piezoelectric film *Int. J. Mech. Sci.* **187** 105915
[7] Bae J-H and Chang S-H 2015 Characterization of an electroactive polymer (PVDF-TrFE) film-type sensor for health monitoring of composite structures *Compos. Struct.* **131** 1090–8
[8] Qing X P, Beard S J, Ikegami R, Chang F and Boller C 2008 Aerospace applications of SMART layer technology *Encyclopedia of Structural Health Monitoring* ed C Boller, F Chang and Y Fujino, 1st edn (Wiley) (https://doi.org/10.1002/9780470061626.shm152)
[9] Haughn K P, Gamble L L and Inman D J 2022 MFC morphing aileron control with intelligent sensing *ASME 2022 Conf. on Smart Materials, Adaptive Structures and Intelligent Systems* (American Society of Mechanical Engineers) p V001T03A013
[10] Sodano H A, Park G and Inman D J 2004 An investigation into the performance of macro-fiber composites for sensing and structural vibration applications *Mech. Syst. Signal Process.* **18** 683–97
[11] Yuan S, Jing H, Wang Y and Zhang J 2024 A whole service time SHM damage quantification model hierarchical evolution mechanism *Mech. Syst. Signal Process.* **209** 111064
[12] Ren Y, Zhang S, Yuan S and Qiu L 2023 In-situ integration and performance verification of large-scale PZT network for composite aerospace structure *Smart Mater. Struct* **32** 055010
[13] Ferreira P M, Machado M A, Carvalho M S and Vidal C 2022 Embedded sensors for structural health monitoring: methodologies and applications review *Sensors* **22** 8320
[14] Janeliukstis R and Mironovs D 2021 Smart composite structures with embedded sensors for load and damage monitoring—a review *Mech. Compos. Mater.* **57** 131–52
[15] Minakuchi S and Takeda N 2013 Recent advancement in optical fiber sensing for aerospace composite structures *Photonic Sens.* **3** 345–54
[16] Lampani L and Gaudenzi P 2018 Innovative composite material component with embedded self-powered wireless sensor device for structural monitoring *Compos. Struct.* **202** 136–41
[17] Lampani L, Sarasini F, Tirillò J and Gaudenzi P 2018 Analysis of damage in composite laminates with embedded piezoelectric patches subjected to bending action *Compos. Struct.* **202** 935–42
[18] Sha F, Xu D, Cheng X and Huang S 2021 Mechanical sensing properties of embedded smart piezoelectric sensor for structural health monitoring of concrete *Res. Nondestr. Eval.* **32** 88–112
[19] Paget C A, Levin K and Delebarre C 2002 Actuation performance of embedded piezoceramic transducer in mechanically loaded composites *Smart Mater. Struct.* **11** 886–91
[20] Mongioì F, Selleri G, Brugo T M, Maccaferri E, Fabiani D and Zucchelli A 2024 Multifunctional composite material based on piezoelectric nanofibers and Cu-CFRP electrodes for sensing applications *Compos. Struct.* **337** 118076
[21] Yin J, Chen S, Wong V-K and Yao K 2022 Thermal sprayed lead-free piezoelectric ceramic coatings for ultrasonic structural health monitoring *IEEE Trans. Ultrason. Ferroelectr. Freq. Control* **69** 3070–80
[22] Philibert M, Chen S, Wong V-K, Liew W H, Yao K, Soutis C and Gresil M 2022 Direct-write piezoelectric coating transducers in combination with discrete ceramic transducer and laser pulse excitation for ultrasonic impact damage detection on composite plates *Struct. Health Monit.* **21** 1645–60
[23] Groo L, Inman D J and Sodano H A 2021 Dehydrofluorinated PVDF for structural health monitoring in fiber reinforced composites *Compos. Sci. Technol.* **214** 108982
[24] Zou X, Zhu R, Chen X, Ran Q and Wang Z 2024 PVDF piezoelectric sensor based on solution blow spinning fibers for structural stress/strain health monitoring *Smart Mater. Struct.* **33** 045006
[25] Liu Q, Li Y, Guan R, Yan J, Liu M, Luo G, Su Z, Qing X and Wang K 2023 Advancing measurement of zero-group-velocity Lamb waves using PVDF-TrFE transducers: first data and application to *in situ* health monitoring of multilayer bonded structures *Struct. Health Monit.* **22** 2641–50
[26] Zhao B, Cheng Z, Zhu Y, Lei L, Wei Z, Ji C, Yu T, Fan J, Yang W and Li Y 2024 Self-diagnosis of structural damage in self-powered piezoelectric composites *Compos. Sci. Technol.* **252** 110619
[27] Raja S and Ikeda T 2008 Concept and electro-elastic modeling of shear actuated fiber composite using micro-mechanics approach *J. Intell. Mater. Syst. Struct.* **19** 1173–83
[28] Raja S, Adya H and Viswanath S 2006 Analysis of piezoelectric composite beams and plates with multiple delaminations *Struct. Health Monit.* **5** 255–66
[29] Giurgiutiu V and Zagrai A 2000 Damage detection in simulated aging-aircraft panels using the electro-mechanical impedance technique *Adaptive Structures and Material Systems* (American Society of Mechanical Engineers) pp 349–58
[30] Gresil M, Yu L, Giurgiutiu V and Sutton M 2012 Predictive modeling of electromechanical impedance spectroscopy for composite materials *Struct. Health Monit.* **11** 671–83
[31] Park G, Cudney H H and Inman D J 2001 Feasibility of using impedance-based damage assessment for pipeline structures *Earthq. Eng. Struct. Dyn.* **30** 1463–74
[32] Raju J, Bhalla S and Visalakshi T 2020 Pipeline corrosion assessment using piezo-sensors in reusable non-bonded configuration *NDT&E Int.* **111** 102220
[33] Li P, Yan J, Cao S and Xu C 2022 Toward on-orbit structural health monitoring of inflatablestructures using electromechanical impedance method *J. Phys.: Conf. Ser.* **2184** 012028
[34] Lu R, Shen Y, Qu W and Xiao L 2022 Health monitoring of high-damping viscoelastic materials using sub-resonator enriched electro-mechanical impedance signatures *Smart Mater. Struct.* **31** 095046
[35] Lu R, Shen Y, Zhang B and Xu W 2023 Nonlinear electro-mechanical impedance spectroscopy for fatigue crack monitoring *Mech. Syst. Signal Process.* **184** 109749
[36] Lu R and Shen Y 2024 Active sensing of industrial fluid degradation via electro-mechanical impedance of a submerged piezoelectric wafer *Smart Mater. Struct.* **34** 015008

[37] Lu R and Shen Y 2024 Entire loosening stage monitoring of bolted joints via nonlinear electro-mechanical impedance spectroscopy *Struct. Health Monit.* (https://doi.org/10.1177/14759217241289872)
[38] Jain A, Minajagi S, Dange E, Bhover S U and Dharanendra Y 2021 Impact and acoustic emission performance of polyvinylidene fluoride sensor embedded in glass fiber-reinforced polymer composite structure *Polym. Polym. Compos.* **29** 354–61
[39] DeAngelis D A and Schulze G W 2016 Performance of PZT8 versus PZT4 piezoceramic materials in ultrasonic transducers *Phys. Proc.* **87** 85–92
[40] Park G, Kabeya K, Cudney H and Inman D 1999 Impedance-based structural health monitoring for temperature varying applications *JSME Int. J. A* **42** 249–58
[41] Bennett J, Shrout T R, Zhang S J, Mandal P, Bell A J, Stevenson T J and Comyn T P 2014 Temperature dependence of the intrinsic and extrinsic contributions in $BiFeO_3$-$(K_{0.5}Bi_{0.5})TiO_3$-$PbTiO_3$ piezoelectric ceramics *J. Appl. Phys.* **116** 094102
[42] Fialka J, Benes P, Michlovska L, Klusacek S, Pikula S, Dohnal P and Havranek Z 2016 Measurement of thermal depolarization effects in piezoelectric coefficients of soft PZT ceramics via the frequency and direct methods *J. Eur. Ceram. Soc.* **36** 2727–38
[43] Mahajan A, Zhang H, Wu J, Ramana E V, Reece M J and Yan H 2017 Effect of phase transitions on thermal depoling in lead-free $0.94(Bi_{0.5}Na_{0.5}TiO_3)$–$0.06(BaTiO_3)$ based piezoelectrics *J. Phys. Chem. C* **121** 5709–18
[44] Annamdas V G M and Soh C K 2010 Application of electromechanical impedance technique for engineering structures: review and future issues *J. Intell. Mater. Syst. Struct.* **21** 41–59
[45] Guo T, Wu L, Wang C and Xu Z 2020 Damage detection in a novel deep-learning framework: a robust method for feature extraction *Struct. Health Monit.* **19** 424–42
[46] Rautela M and Gopalakrishnan S 2021 Ultrasonic guided wave based structural damage detection and localization using model assisted convolutional and recurrent neural networks *Expert. Syst. Appl.* **167** 114189
[47] Giurgiutiu V and Zagrai A 2005 Damage detection in thin plates and aerospace structures with the electro-mechanical impedance method *Struct. Health Monit.* **4** 99–118
[48] Giurgiutiu V and Zagrai A 2000 Characterization of piezoelectric wafer active sensors *J. Intell. Mater. Syst. Struct.* **11** 959–76
[49] Soh C K, Tseng K K-H, Bhalla S and Gupta A 2000 Performance of smart piezoceramic patches in health monitoring of a RC bridge *Smart Mater. Struct.* **9** 533